

# Laser Transmission Welding of Thermoplastics—Part II: Experimental Model Validation

**James D. Van de Ven**  
e-mail: vandeven@me.umn.edu

**Arthur G. Erdman**  
e-mail: agerdman@me.umn.edu

Mechanical Engineering Department,  
University of Minnesota,  
111 Church Street SE,  
Minneapolis, MN 55455

*Two laser transmission welding experiments involving polyvinyl chloride are presented that aim to validate a previously presented welding model while helping to further understand the relationship between welding parameters and weld quality. While numerous previous research papers have presented the results of laser welding experiments, there exists minimal work validating models of the welding process. The first experiment explores the interaction of laser power and welding velocity while the second experiment explores the influence of clamping pressure. Using the weld width as the primary model output, the agreement between the welding experiments and the model have an average error of 5.6%. This finding strongly supports the validity of the model presented in Part I of this two paper set (Van de Ven and Erdman, 2007, ASME J. Manuf. Sci. Eng., 129, pp. 849–858). Additional information was gained regarding the operating window for laser transmission welding and the thermal decomposition of polyvinyl chloride. Clamping pressure was found to provide a small, but not statistically significant, influence on the visual appearance, weld width, and weld strength. [DOI: 10.1115/1.2752832]*

*Keywords:* laser welding, modeling, PVC

## Background

Due to the complexity of modeling the heating phase of laser transmission welding, a good deal of work has utilized experimental methods to study welding parameters. While purely experimental work provides important findings to the field, the primary purpose of the laser welding experiments presented in this paper is to validate a mathematical model of laser transmission welding presented in Part I of this series [1]. Within the literature very few welding experiments have been used for the purpose of model validation.

In 2002, F. Becker and H. Potente, University of Paderborn, presented a comparison of results between their finite element model of the heating phase of laser transmission welding and experimental welding data. To achieve better agreement between the weld data and the model, the model was modified by hypothetically varying the absorption coefficient with temperature. The absorption coefficient, as a function of temperature, was predicted to follow the same curve as the material density [2]. Using experimental methods, the author found the opposite of this relationship between the absorption coefficient and temperature [3]. It is interesting to note that in the experiments by Becker and Potente, the dependent variable of their finite element model—temperature—was not measured. Instead, temperature was inferred by the depth of the melt layer in the weld.

A second attempt at validating a model with welding experiments was presented in 2002 by Kennish et al. In this work a very simplified model is used to predict a weld interface temperature of 305°C for a specific set of operating conditions. The validation experiment uses thermocouples to directly determine the interface temperature. In this case, the temperature reading of the thermocouple indicated an interface temperature of 705°C [4]. This large deviation is mostly due to direct absorption of the laser radiation by the thermocouple.

## Temperature Measurements

The primary output from the mathematical model of laser welding is the temperature distribution in the weld zone as a function of time. The best way to validate the model would be to directly measure the temperature in the weld zone. Unfortunately, measuring this subsurface temperature is difficult.

One possible method of measuring the material temperature directly is through the use of a thermocouple or thermistor. Unfortunately, as discussed by Becker and Potente and demonstrated by Kennish et al., thermocouples will absorb the laser energy directly and not correctly read the temperature of the surrounding material [2,4]. In addition, placing an object in the weld zone that is in contact with both the “absorptive” and “transmissive” parts will likely affect the desired clamping pressure or even cause a gap between the two materials.

Another possible method to measure the temperature in the weld zone is using an infrared pyrometer. If the operating frequency of the pyrometer is at a wavelength of high transmission through the “transmissive” material, a signal from the surface of the “absorptive” part can be detected. To operate in this manner, the emissivity of the “transmissive” part needs to be known. Unfortunately, work in this area has found emissivity measurements to be highly imprecise [2].

Despite the difficulty determining the emissivity of a thermoplastic material, pyrometers have been used in laser welding applications for various purposes. Baylis et al. used a radiation pyrometer operating at 1800 nm to measure the weld zone temperature during welding. In the work it is noted that the temperature readings are relative, not absolute, because of the difficulty in calibrating the pyrometer. In addition, the pyrometer readings showed a great deal of scatter between samples run at the same test conditions [5].

Herzog et al. demonstrate a second application of infrared pyrometry for use in feedback control when laser welding polymers to natural fiber composites. Due to the inhomogeneity of the natural fibers within the composites, inconsistent welds were created as a result of changes in the absorption coefficient of the “absorbing” part. To create a more uniform weld, a laser pyrometer, operating at 2 μm was used as a feedback sensor in a control loop.

Contributed by the Manufacturing Engineering Division of ASME for publication in the JOURNAL OF MANUFACTURING SCIENCE AND ENGINEERING. Manuscript received April 17, 2007; final manuscript received May 3, 2007. Review conducted by Kornel F. Ehmann.

It was also noted in this work that the readings from the pyrometer were relative because no calibration was conducted [6].

Because of the difficulty measuring the temperature within the weld zone, the width and depth of the weld are often used as a measured output of welding experiments. This can be accomplished by direct measurement or through the use of a microscope. A number of different researchers have used a microtome to create thin slices (15–30  $\mu\text{m}$ ) of the weld area, which are analyzed under an optical microscope [2,7,8]. The weld width and depth can be compared with the melting temperature of the thermoplastic and the temperature profile predicted by the model, allowing model validation.

A prime interest to many applications of welding thermoplastics is the weld strength. The weld strength is occasionally measured using a lap-shear test, which provides a measure of the shear strength of the material [5,6]. More commonly, a measure of tensile strength is desired, which is often accomplished through the use of a T-joint sample. In the T-joint geometry the “transmissive” material is the top of the T and the “absorptive” material forms the stem of the T. The laser beam is passed through the top of the T and absorbed in the stem [9–11]. This geometry allows simple fixturing of the sample in a loadframe to measure the joint strength. For both of these methods the weld width and length should also be measured to allow the failure strength to be calculated.

### Pressure in the Weld Zone

As discussed in Part I of this set of papers [1], the pressure in the weld zone is important as it directly affects the contact conduction between the two materials being joined. While the importance of joining pressure has not been explored by other researchers through modeling, some experimental work in this area can be found. It should be noted that in all of the sources cited below, the pressure discussed is due to external clamping, while the internal pressure due to thermal expansion, as discussed in the model in the first paper, was not monitored.

Work presented by Potente et al. in 2001 explored the relationship between clamping pressure and joint strength when welding the thermoplastic PEEK. Their experiment varied the clamping pressure between 1 MPa and 3 MPa. The results demonstrated that maximum weld strength occurs at 1.5 MPa of clamping pressure. However, the authors conclude that, due to the large error bars relative to the differences in weld strength, the effect of pressure is negligible in the testing range [11]. These data have an average error of approximately 12 N/mm<sup>2</sup>, while the total difference between the highest average strength and the lowest average strength is approximately 2 N/mm<sup>2</sup>.

In 1999, Grewell presented data relating weld strength to clamping pressure. The results of these data indicate that the maximum weld strength occurs at 2.2 MPa of clamping pressure. Above this pressure the data indicate a significant decrease in weld strength. Grewell explains this significant decrease as a result of shear thinning of the melted polymer in the weld zone [12]. It should be noted that the error bars for these data are also quite large with an average error of approximately 7.5 MPa and a total difference between the highest strength and the lowest average strength of approximately 15 MPa.

### Laser Welding System

The laser system used for the experiments presented in this paper uses a 30 W 808 nm diode laser bar that is conductively cooled using a Peltier cooler. The diode bar is coupled to a 2-m-long 1.1-mm-diameter fiber optic cable with an output lense assembly that is kept clear of dust and debris by a positive airflow nozzle. The laser spot diameter is adjustable between 2 mm and 10 mm by moving a slide that changes the distance between the optic head and the working surface. The laser is powered by a 2 V power supply that operates at up to 50 A. The laser head is

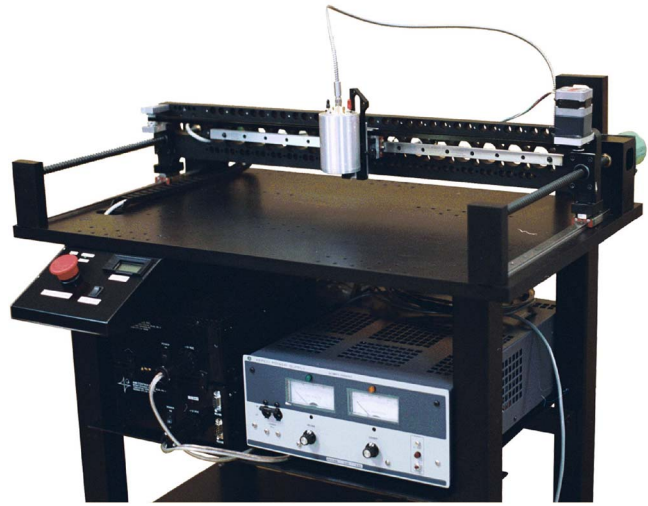


Fig. 1 Diode laser system, which utilizes an  $x$ - $y$  gantry table (photo courtesy of Aim Controls)

mounted on an  $x$ - $y$  gantry table with encoder feedback on both axes. A photograph of this system can be found in Fig. 1.

### Laser Welding Experimental Setup

The two principal options for the geometry of laser transmission welding samples are a lap weld and a T-joint. The major reason to choose one geometry over the other is the desired method of testing weld strength. Lap weld geometry is best suited to a lap-shear test, while a T-joint geometry is best suited to a direct tensile strength test. As found in other areas of material testing, typically tensile strength test data are more accurate and repeatable than shear strength test data [13]. For this reason, a T-joint geometry was selected. This joint also allowed the weld zone to be fully contained, preventing any squeeze-out, or welding flash.

The dimensions of the two parts composing the T-joint geometry are selected based on the intentions of the study. This research project primarily focuses on designing subsurface lap welds, thus there is little interest in welding conditions when operating near the edge of a part where material “squeeze out” is likely. This dictates that the stem of the T-joint needs to be thicker than the widest weld expected. For a model design example presented in Part I of this series, a target was set for a 2.5-mm-wide weld. With the expectation of possibly desiring to increase the width during various experiments, a width of 6.4 mm was selected for the stem of the T-joint. The thickness of the “transparent” part forming the top of the T-joint needs to balance minimizing material usage and maintain adequate stiffness to minimize bending during tensile strength testing where load is applied to the outer wings of the “transparent” part. This balance is met with a 3.2-mm-thick specification for the “transparent” part. Finally, 25 mm was set for the length of the T, along the direction of laser travel. This dimension allows adequate length of weld for assessment. A summary of the specimen geometry and dimensions can be found in Fig. 2.

The two parts forming the T-joint are Type I polyvinyl chloride (PVC) from K-mac Plastics<sup>1</sup> and were cut from extruded sheet and machined to final dimensions. Despite attempts to maintain consistency during machining, the surface finish of the machined surfaces is not identical for all samples. Because the contact conduction is inversely proportional to the surface roughness, the variation in roughness cannot be overlooked. The roughness of the

<sup>1</sup>K-Mac Plastics, 3821 Clay Ave. SW, Wyoming, MI 49548.

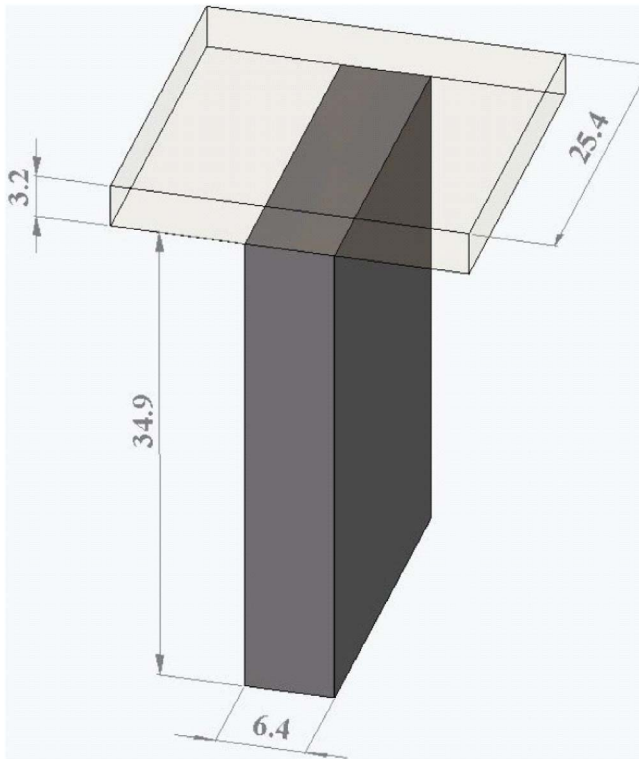


**Fig. 2** T-joint geometry with the associated dimensions in millimeters. The “transparent” part forms the top of the T, while the “absorptive” part forms the stem of the T.

top surface of the “absorptive” parts was measured using a surface roughness tester, the Surtronic 10, manufactured by Taylor-Hobson. The root mean square roughness of these surfaces ranged between  $1.0\ \mu\text{m}$  and  $2.5\ \mu\text{m}$ . The samples were placed in groups with other samples of similar roughness. The two individual experiments presented here use only one surface roughness group, minimizing noise in the experiment. It should also be noted that the surface of the “transmissive” parts, which contacts the measured surface, is an extruded surface and routinely measures between  $0.0\ \mu\text{m}$  and  $0.1\ \mu\text{m}$  of roughness.

A fixture was developed to repeatedly locate the samples during welding while allowing the clamping pressure to be varied. The base of the fixture contains a machined slot where an end of the “absorptive” part is placed, holding the stem of the T-joint in a vertical position. The transparent part is placed horizontally on top of the “absorptive” part and held in place by a rotating carriage, which is attached to a pair of rotating arms. At the end of the arms, force is applied by a precision helical compression spring. By using springs of varying stiffness and varying the spring deflection, the clamping pressure on the welding joint can be controlled. This fixture can be seen as a solid model in Fig. 3, while

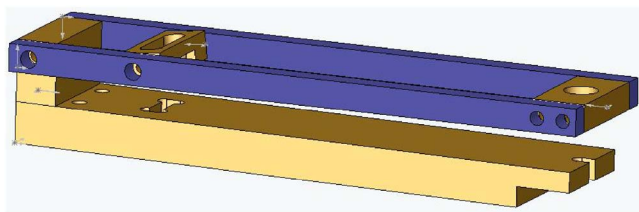


**Fig. 3** Solid model of the welding fixture used to create the T-joint geometry



**Fig. 4** Photograph of the welding fixture mounted to the welding table. A description of the fixture based on the lower figure: the arms pivot at the far right of the photograph. The “absorbing” part is placed in a slot approximately 2 in. from the pivot and the “transparent” part is placed on top of this part in a T-joint. This “transparent” part is held in place by a rotating carriage, which is the second pivot on the pair of arms. On the far left side of the arms, a precision spring is used to apply pressure. By compressing the spring a specified amount, a known load is applied, allowing the clamping pressure in the weld zone to also be known.

photographs of the machined assembly can be found in Figs. 4 and 5.

The carriage above the “transparent” part not only transmits force to the joint, but also has a machined slot to allow the laser beam to irradiate the sample for a length of 19.1 mm. The slot in the carriage is designed to create contact with the “transparent” part directly over the “absorptive” part outside of the slot area, as well as to the sides of the slot. The purpose of this design decision was to minimize bending in the “transmissive” part, creating more uniform contact in the welding zone.

Five different precision helical springs are used to apply force to the end of the arms of the welding fixture. The measured spring

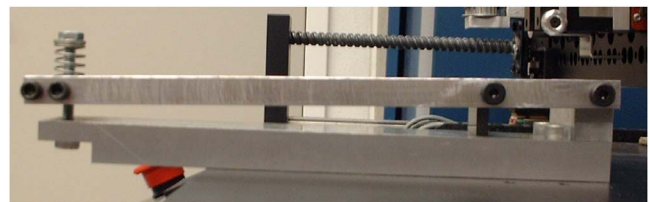


**Fig. 5** Photograph of the welding fixture mounted to the welding table. A description of the fixture based on the lower figure: the arms pivot at the far right of the photograph. The “absorbing” part is placed in a slot approximately 2 in. from the pivot and the “transparent” part is placed on top of this part in a T-joint. This “transparent” part is held in place by a rotating carriage, which is the second pivot on the pair of arms. On the far left side of the arms, a precision spring is used to apply pressure. By compressing the spring a specified amount, a known load is applied, allowing the clamping pressure in the weld zone to also be known.

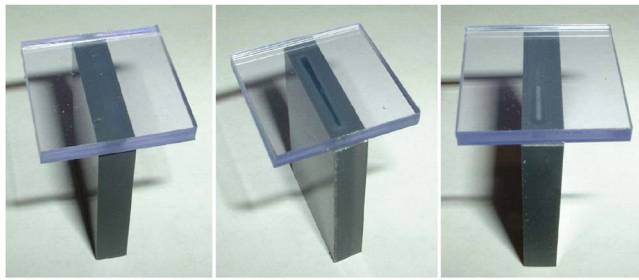


**Fig. 6 Fixture and grip used to determine the weld failure force of the T-joint samples**

rates of these springs vary from 0.946 N/mm (5.40 lb/in.) to 7.311 N/mm (41.75 lb/in.). Using one of the five different springs, the pressure in the weld zone can be set to any value between 50 kPa and 4000 kPa (7.25 psi and 580 psi).

A set of parameters were designed for all the welding experiments, which aim to minimize variation. First, the PVC samples are sheared from large sheets into sizes slightly larger than the final dimensions. The samples are then machined to size in a manual vertical mill. As previously discussed, the samples are then sorted by surface roughness. Just before welding, the contacting surfaces of the “transparent” and the “absorptive” parts are cleaned with a cotton swab containing an isopropyl alcohol and water mixture. The purpose of cleaning the surfaces is to remove any oil from handling or machining that might interfere with the integrity of the weld. The samples are then placed in the welding fixture.

In the experiments described in this paper, the laser system was run in a vector mode using the computer interface. In this mode, the laser head starts at the location that the laser will begin firing. The optic head, mounted to the *x-y* gantry, moves 25 mm in the opposite direction of the weld to create a ramp distance. The optic head then accelerates to the specified velocity and the laser is powered at the initial starting location. The optic head continues to move at the specified velocity while traveling across the sample. The power to the laser is then interrupted and the optic head ramps down to zero velocity before returning to the initial position. To minimize the effect of any possible power spikes while first powering the laser, the initial position is set to 75 mm away from the sample being welded. Along this initial travel area, a concrete backer board is placed on the welding table to absorb the laser power.

Following welding, the samples are assessed by three different measurements. First, a visual inspection is used to determine if thermal decomposition can be detected. Visual inspection also yields information about the weld width consistency and any possible anomalies. Second, a tensile test, using a custom grip and fixture, is used to determine the force required to fail the weld. Finally, the width of the weld is measured with a caliper, which allows the area of the weld to be calculated and the failure strength to be determined.

Visual inspection monitored the consistency of the welds and looked for evidence of decomposition. The welds were classified in one of the following manners: no weld, narrow weld, tapering weld, good weld, slight burn, moderate burn, and heavy burn. A “good” weld is characterized by a uniform looking weld that shows no sign of thermal decomposition. Photographs of a “good” weld, a “tapering” weld, and a “decomposed” weld can be found in Fig. 6.

The tensile test loaded the welds in tension to the point of failure. This test was conducted in an MTS electro-mechanical loadframe at a displacement rate of 1.25 mm/min (0.05 in./min) using a 1000 N (225 lbs) loadcell. The quantitative measure from this test is the failure force, which is defined as the maximum load reached during the tensile test.

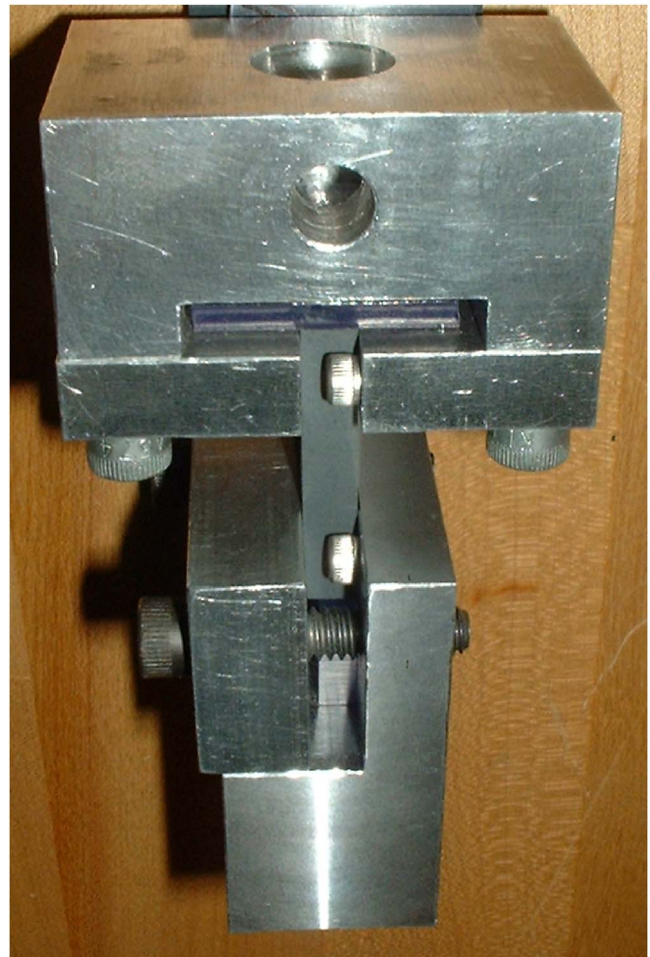


**Fig. 7 Examples of three different visual ratings for the welded “T” samples. The left photo receives an aesthetic “good” rating. Note the uniform weld that is free of any visual signs of thermal decomposition. In the center photo, the weld exhibits decomposition along the centerline and receives a “medium decomposition” rating. The weld on the right receives a “tapering” rating as the weld starts at a decent width, but the width tapers toward the far side of the sample. For reference, the aesthetic quality is not fully captured in these photographs and is much easier to distinguish directly from the samples.**

A grip and fixture were designed to apply the tensile force to the weld samples in the loadframe. The top fixture is essentially an inverted “t-slot” where the “transparent” part slides into a horizontal slot, and the “absorptive” part extends vertically down out of the slot. The other end of the “absorptive” part is clamped in a simple grip that uses two socket head cap screws to apply a clamping force.

To assure repeatable strength results, the sample needs to be precisely aligned in the fixture and grip. Holes are tapped in both parts, allowing the heads of No. 6-32 socket head screws to provide horizontal alignment, assuring the samples were placed directly in the center of the grips. The bottom of the “T” specimen fully contacts a shim in the lower grip, forcing the sample to be square in the fixture. To create contact with the shim during setup, a spring is placed in the upper fixture to press the specimen down into the lower grip. A photograph of the fixture and grip with a T-joint sample can be found in Fig. 7.

Following the tensile test, the width of the weld was measured. The weld width, which was visually apparent on the “absorptive”

parts, was measured using a caliper. In the case of a varying weld width across the length of the weld, an average of the width at the two ends was reported.

### Welding Experiments

Two experiments were run using the laser welding system. The first of these experiments explores the relationship between laser power and welding velocity, while all other variables are held constant. The second experiment explores the influence of clamping pressure at a laser power and weld velocity that were found to produce good welds in the first experiment.

### Experimental Procedure: Laser Power and Velocity

As discussed, a prime purpose for conducting laser transmission welding experiments is to validate the model presented in the first paper of this set, while simultaneously gaining a better understanding of the influence of the input parameters on weld results. In the paper presenting the model, a design example was presented that developed the parameters necessary to create a 2.5-mm-wide weld between two PVC parts, one clear and the other gray [1]. The design solution specifies a laser power of 17 W, a 5.7-mm-diameter laser beam, a weld velocity of 0.06 m/s (2.4 in./s), and a clamping pressure of 2.0 MPa (290 psi). Using these design parameters the model predicts a weld width of 2.60 mm.

To validate the model, an experiment was designed containing two crossed factors: laser power and travel velocity, each with four levels. The ranges of the two factors center near the parameters determined by the design example. The laser power is varied between 16 W and 19 W in steps of 1 W, while the travel velocity ranges between 0.04 m/s and 0.07 m/s in steps of 0.01 m/s. To provide adequate replication, each subgroup contains five samples. For this specific experiment, all other welding parameters remain constant. In summary, the experiment is a 4 × 4 factorial with five replications of each factor level combination, for a total of 80 samples.

Attempts were made to minimize the influence of noise variables in this experiment. First, the “absorptive” parts selected all had a measured surface roughness between 1.7 μm and 2.1 μm. Second, the run order for the experimental units was completely randomized. Third, the clamping pressure was checked for each sample to minimize any possible variation. Forth, all experiments were run in a continuous 2 h period to minimize any day-to-day variation. Finally, all samples were cleaned prior to welding.

### Results: Laser Power and Velocity

All 16 combinations of laser power and welding velocity resulted in some form of weld between the “absorptive” and “transmissive” parts. These welds were assessed by three different means including: visual inspection, weld tensile force at failure, and weld width. This section will present the results of these three assessments.

The majority of the samples from this experiment earned a visual inspection rating of “good.” The visual ratings were transformed into a pattern coding as can be seen in Table 1. As can be noted in this table, welds formed at high laser power and low weld velocity, such as 19 W and 0.04 m/s, resulting in decomposition. At the other end of the spectrum, welds formed at low laser power and high weld velocity, such as 16 W and 0.07 m/s, resulting in thin or tapering welds.

As described in the Laser Welding Experimental Setup portion of the text, all samples were subjected to a destructive force test. The average maximum force during the destructive test of the five replications of each factor level combination and the standard error can be found in Table 1. The standard error is the standard deviation divided by the square root of the number of samples.

Following the tensile test, the width of the weld, as visually apparent on the “absorptive” part, was measured. The weld widths

**Table 1 Averaged weld failure force and the visual ratings for each of the factor level combinations. As described by the color code on the right side of the table, each color represents a different level of visual appearance.**

Averaged Failure Force (N)		Power (W)				Color Key
		16	17	18	19	
Velocity (m/s)	0.04	493	585	736	636	<div style="display: flex; flex-direction: column; gap: 5px;"> <div><span style="color: cyan;">■</span> narrow weld</div> <div><span style="color: green;">■</span> good weld</div> <div><span style="color: gray;">■</span> slight burn</div> <div><span style="color: black;">■</span> moderate burn</div> </div>
	0.05	438	609	580	601	
	0.06	196	202	406	223	
	0.07	20	86	137	140	

Standard Error - Failure Force (N)		Power (W)			
		16	17	18	19
Velocity (m/s)	0.04	72	46	139	137
	0.05	64	62	61	41
	0.06	30	33	96	63
	0.07	14	36	42	33

were found to vary between 2.00 mm (0.079 in.) and 3.18 mm (0.125 in.). The average of the five replications of each factor level combination can be found in Fig. 8. From this plot it can be noted that the widest welds occurred in combinations of high laser power and low weld velocity, while narrower welds occurred in combinations of low laser power and high weld velocity. These data and the standard error for each factor level combination can also be found in Table 2.

Altering the laser power and welding velocity ultimately varies the laser energy per unit of weld length. This quantity, line energy, is defined as the laser power divided by the laser velocity, creating units of Joules per millimeter. To give an alternative perspective, the weld width data presented in Fig. 8 and Table 2 are represented as a function of the line energy in Fig. 9.

Due to the significant variations in weld width between all the factor level combinations, it is more advantageous to compare the weld strength than simply the force at failure. The weld strength can be calculated by dividing the failure force by the measured weld width times the weld length, which is known to be 19.1 mm (0.750 in.). The average calculated weld strength for each factor level combination is found in Fig. 10 and the weld strength as a function of the line energy is found in Fig. 11. Generally, stronger welds are achieved at higher levels of line energy.

### Discussion: Laser Power and Velocity

The laser power and weld velocity experiment provided both model validation and further understanding of the relationship be-

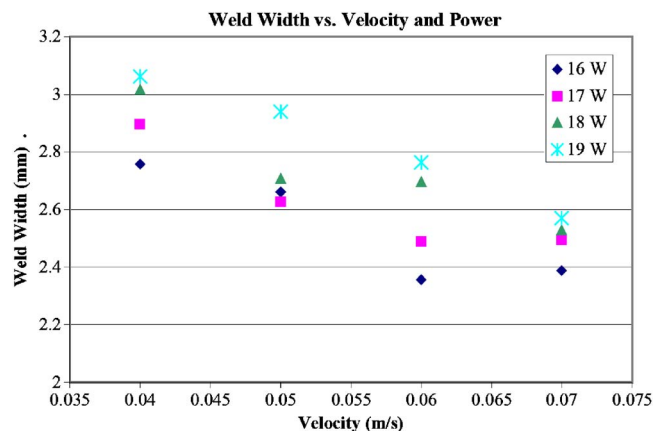


**Fig. 8 Weld width as a function of velocity and laser power**

**Table 2 Weld width as a function of velocity and laser power in a tabular format**

Averaged Weld Width (mm)					Standard Error - Weld Width (mm)				
Velocity (m/s)	Power (W)				Velocity (m/s)	Power (W)			
	16	17	18	19		16	17	18	19
0.04	2.76	2.90	3.02	3.06	0.04	0.07	0.04	0.07	0.06
0.05	2.66	2.63	2.71	2.94	0.05	0.04	0.06	0.04	0.02
0.06	2.36	2.49	2.70	2.76	0.06	0.16	0.11	0.05	0.03
0.07	2.39	2.49	2.53	2.57	0.07	0.12	0.03	0.05	0.06

tween input parameters and weld quality. This relationship can be used in conjunction with the model to understand the temperature necessary to create a weld, while avoiding thermal decomposition. In addition, further insight is gained regarding the consistency of the three assessment methods: visual appearance, failure force, and weld width.

This experiment provides evidence that strongly supports the heating phase model presented in Part I of this series. In the design example presented in Part I of this series, a 2.60-mm-wide weld was predicted with welding parameters of 17 W of laser power, a laser beam diameter of 5.7 mm, a weld velocity of 0.06 m/s, a clamping pressure of 2.0 MPa, and a surface roughness of 1.8  $\mu\text{m}$ . In the welding experiment replicating these conditions, the average weld width of five replications is 2.49 mm

with a standard error of 0.11 mm. The error between the width predicted by the model and the width found in the experiment is 4.3%, indicating that the model appears to be predicting weld conditions accurately. For reference, within the field of laser transmission welding, Becker and Potente came closest to verifying their model with findings of approximately 10–12% error, after adjusting their model based on the experimental results [2].

To further verify the agreement between the model and the experimental results, models were run for the majority of the other factor level combinations. The predicted weld width from the results of these models, the measured weld width, and the error between the two values can be found in Table 3. Note that the factor level combinations of 18 W and 19 W at 0.04 m/s resulted in temperatures that exceeded 1000 K within the core of the material. The model is designed to interpolate values up to 1000 K and thus these two factor level combinations, which both result in thermal decomposition, were not modeled. The average error for

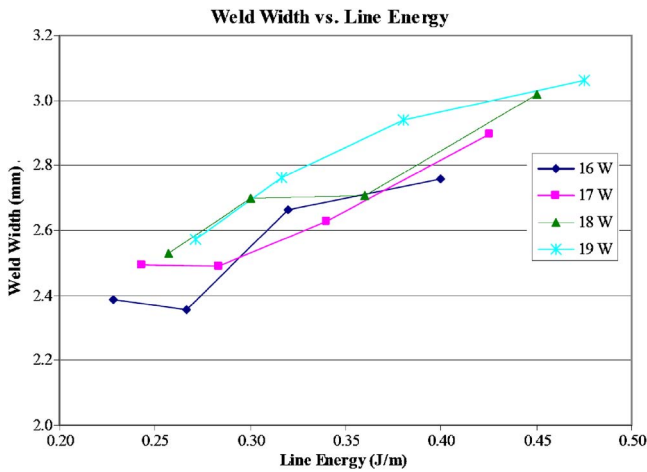


**Fig. 9 Average weld width as a function of line energy, defined as the laser power divided by the welding velocity**

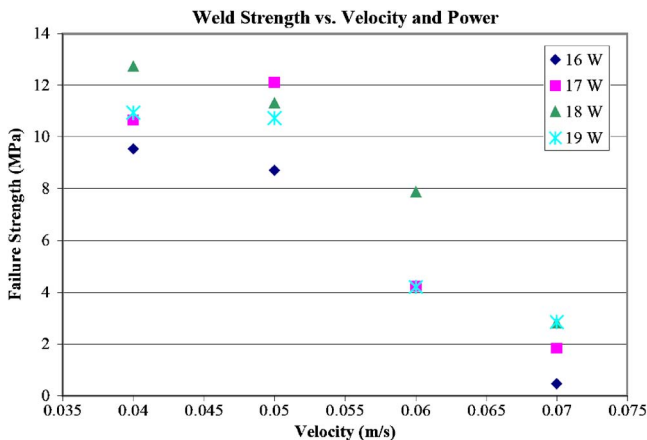


**Fig. 10 Calculated weld strength as a function of velocity and laser power**

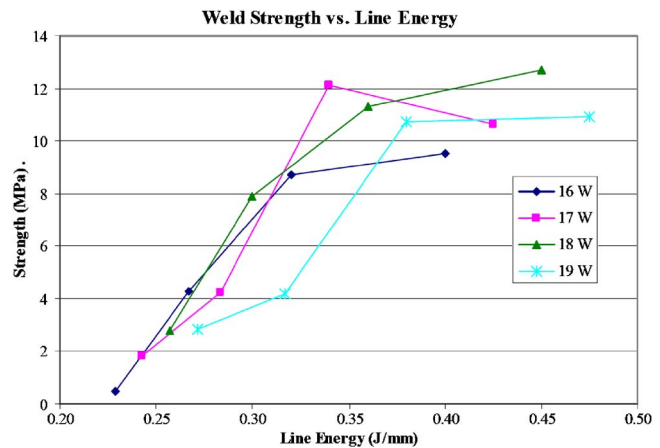


**Fig. 11 Calculated weld strength as a function of line energy**

**Table 3 Table of the weld width predicted by the model, the weld width measured in the experiment, and the error between the two values**

Velocity (m/s)	Weld Width (mm)	Power (W)			
		16	17	18	19
0.04	Predicted	3.08	3.18		
	Measured	2.76	2.90	3.02	3.06
	Error	10.4%	8.9%		
0.05	Predicted	2.80	2.90	2.98	3.04
	Measured	2.66	2.63	2.71	2.94
	Error	4.9%	9.4%	9.1%	3.3%
0.06	Predicted	2.48	2.60	2.72	2.84
	Measured	2.36	2.49	2.70	2.76
	Error	5.0%	4.3%	0.8%	2.7%
0.07	Predicted	2.20	2.32	2.44	2.56
	Measured	2.39	2.49	2.53	2.57
	Error	8.5%	7.5%	3.7%	0.4%

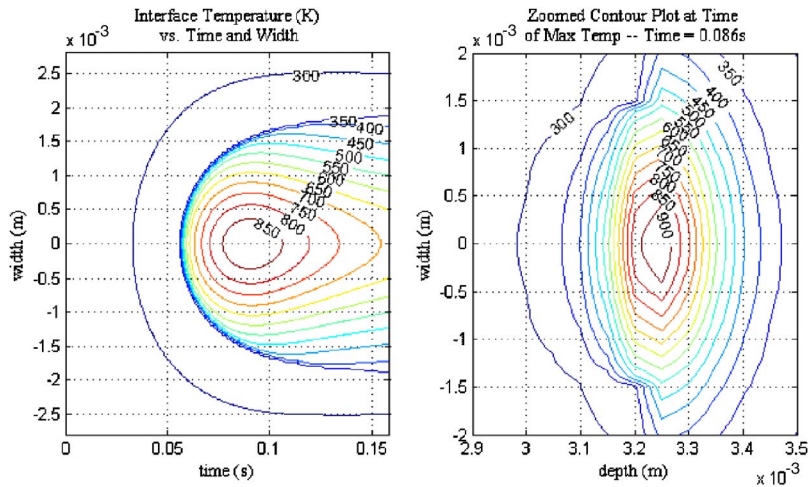


**Fig. 12 Model output of the factor level combination of 19 W and 0.05 m/s. The samples welded at this condition did display slight thermal decomposition.**

the 14 factor level combinations is 5.6%. The variation in error is likely the result of the relatively small sample size for each factor level combination.

Analyzing the weld width at the various factor level combinations clearly indicates that weld width increases with increasing laser power and decreasing weld velocity. When the weld width data are presented in terms of line energy, as in Fig. 8, the trend is even more apparent. Another interesting finding, which can be observed in Table 2, is that the standard error of the replications of each factor level combination are small, ranging between 0.7% and 6.7% of the measured value. Although temperature in the weld zone would be the measured output that ideally validates the model, as previously discussed, the consistent measure of weld width provides confidence that it is a suitable substitute.

Aesthetics of the welded joint are important to certain applications, yet the visual appearance of the weld also provides other important information about the weld. First, as can be seen from Table 1, it is apparent that the processing window for creating a visually pleasing weld is sizeable. In this experiment, 11 of the 16 factor level combinations received a visual rating of “good.” Second, visual inspection allows quick identification of process parameters that lead to thermal decomposition. By running the model at the conditions that caused decomposition, understanding is gained of the temperature and time of exposure that create thermal decomposition. To illustrate this point, a model simulation was run at one set of parameters that resulted in decomposition in this experiment.

One of the factor level combinations where slight decomposition was noted was at 19 W of power and a velocity of 0.05 m/s. The model is used to better understand the temperature profiles within the two parts at this welding condition. Inputs to the model include: power=19 W, velocity=0.05 m/s, beam diameter=5.7 mm, surface roughness=1.8  $\mu\text{m}$ , and clamping pressure=2.0 MPa. In addition, the timestep for this model is set to 0.5 ms with a run time of 0.16 s and a distance between each node of 0.02 mm. The mesh Fourier number for this condition is 0.024, indicating stable operation, designated by values below 0.5. The output from this model can be found in Fig. 12.

The model of this factor level combination provides important information about the temperature profile that results in thermal decomposition. The plots in Fig. 12 and the raw output from the model indicate that the maximum subsurface temperature reaches 948 K while the maximum temperature at the interface reaches 889 K. It can also be noted that the elapsed time at these elevated temperatures is short. It is reasonable to predict that due to the

autocatalytic nature of PVC, if the exposure time were increased by welding at a lower velocity, the temperature resulting in the onset of decomposition would decrease.

In many industrial applications, the weld strength is one of the most important joint characteristics. The model presented in Part I of the series predicts that a weld is created when the interface temperature exceeds 485 K, while not exceeding a temperature that causes decomposition; in no way does the model predict the strength of the weld created. This experiment varying laser power and weld velocity does provide insight into the conditions influencing weld strength.

As noted in the “Results: Clamping Pressure” section, the weld strength shows a clear increase with increasing line energy. This increase in weld strength with increasing line energy is more abrupt at lower levels of line energy. Near the upper levels of line energy, factor level combinations of high power and low velocity, the increase in weld strength is less apparent. These samples welded at high line energy levels are conditions where visual decomposition occurred. From this information it is logical to conclude that optimal weld strength is produced by raising the temperature in the weld zone to just below a temperature resulting in decomposition.

It should be noted, that the welds in the T-joint samples are subject to stress concentrations at the edge of the weld line. The weld widths demonstrated in this work are smaller than the stem of the T in order to prevent extrusion of melted polymer, or flash, outside of the T-joint geometry. Because the welds are not at the full width of the stem of the T, the edges of the weld are subjected to stress concentrations when pulled in the loadframe. These stress concentrations are affecting the calculated weld strength.

### Experimental Procedure: Clamping Pressure

A second experiment was designed to explore the influence of clamping pressure on weld quality. This experiment contains one factor, clamping pressure, which is varied between 0.5 MPa and 4 MPa in graduations of 0.5 MPa. For this experiment, the power is held constant at 17 W, the welding velocity is held at 0.06 m/s, and the laser beam diameter is set to 5.7 mm. These parameters match the design example presented in the first paper of this series. To provide sufficient replication, eight samples were run at each of the eight pressure conditions, for a total of 64 samples.

As in the laser power and weld velocity experiment, extensive attempts were made to minimize the noise variables. The measured roughness of welding surface of the “absorptive” parts

**Table 4** Averaged weld failure force and the visual ratings for each of the pressure levels. As described by the color code on the right side of the table, each color represents a different number of occurrences of tapered welds within each subgroup of eight. Note that no visual decomposition occurred in any of the samples during this experiment.

Pressure	0.5	1.0	1.5	2.0	2.5	3.0	3.5	4.0	Color Key
Failure Force (N)	255.2	255.4	261.9	237.6	304.5	277.9	293.8	309.7	good welds
Standard Error (N)	37.6	55.1	48.7	37.8	50.4	38.6	28.6	58.6	1/8 tapered
									2/8 tapered
									3/8 tapered

ranged from 1.4  $\mu\text{m}$  to 1.6  $\mu\text{m}$ . The run order for samples was completely randomized. All samples were welded on the same day to minimize any possible day-to-day variation. Finally, all samples were cleaned prior to welding.

### Results: Clamping Pressure

All 64 samples in this experiment produced a weld between the two PVC parts. As in the previous experiment, these samples were assessed by three methods: the visual appearance, the maximum tensile force at failure, and the measured width of the weld. However, in contrast to the previous experiment, the variations between subgroups in this experiment were more subtle.

All samples from this experiment created welds that showed no visible thermal decomposition. With few exceptions nearly all of the samples were given a visual “good” rating. When welding at pressures of 2.5 MPa or below, between one and three samples of the eight from each subgroup exhibited a slightly tapering weld. The distribution of samples with visual tapering included three at 0.5 MPa and 1.0 MPa, two at 1.5 MPa and 2.0 MPa, and one at 2.5 MPa. The aesthetic weld ratings can also be found in Table 4.

Following the visual inspection, all samples were placed in the loadframe and pulled in tension at a strain rate of 1.25 mm/min (0.05 in./min). The measured outcome from this destructive test is the maximum force during the test. The average failure force and standard error for each factor level can be found in Table 4. The average failure force varied between 237.6 N and 309.7 N.

After the tensile test, the weld width was measured directly on the “absorptive” parts. The average measured widths varied between 2.65 mm (0.104 in.) and 2.74 mm (0.108 in.), creating quite small variation between factor levels. A plot of the average width for each factor level and error bars corresponding to the standard error can be found in Fig. 13. It can be noted from the plot that a step increase in the weld width occurs when transitioning between samples welded at or below 2.0 MPa and samples welded above this pressure.

To provide a more uniform method of comparing the factor levels, the failure force is divided by the weld area to obtain an ultimate strength. The area of the weld is obtained by multiplying the measured width by the 19.1 mm (0.750 in.) weld length. The

average weld strength for each factor level and the corresponding standard error can be found in Fig. 14. Note that while the error bars are relatively large compared to the differences between the factor levels, there does again appear to be an increasing step in strength above 2.0 MPa.

### Discussion: Clamping Pressure

Analyzing the data from the welding experiment involving varying the clamping pressure provides some important insights. Foremost, this experiment demonstrates that welds can be successfully created at clamping pressures between 0.5 MPa and 4.0 MPa. Within this pressure range, distinctions can be made when evaluating the visual appearance, weld width, and strength. Generally speaking the data form a favorable improvement in weld quality between 2.0 MPa and 2.5 MPa, based on the three assessment criteria.

The visual consistency of the welds is found to be dependent on the clamping pressure. All samples welded at pressures above 2.5 MPa showed no visual sign of tapering, or decreasing of the weld width across the sample. At levels of lower pressure, a greater percentage of the replications of each subgroup exhibited a tapering weld. At the lowest pressure level, 0.5 MPa, three of the eight samples demonstrated tapering. The inconsistent visual appearance of the welds formed at the lower levels of pressure not only has meaning for applications of this technology where aesthetics of the weld are important, but also raises concern over the integrity of the welds.

As with the visual assessment, the measured weld width also varies with pressure. The weld width data show an increase between 2.0 MPa and 2.5 MPa, with a slight decline in the average weld width above 2.5 MPa. It should be noted that the differences between the mean of each factor level are not large with respect to the standard error, especially at the higher levels of pressure, which prevents statistically supported conclusions. Despite this fact, the average weld width at 2.5 MPa is substantially higher than at 0.5 MPa, with no overlap in the error bars, indicating a significant difference between the factor levels.

Unlike both the visual appearance and the measured weld width, there is no significant variation in the weld strength across

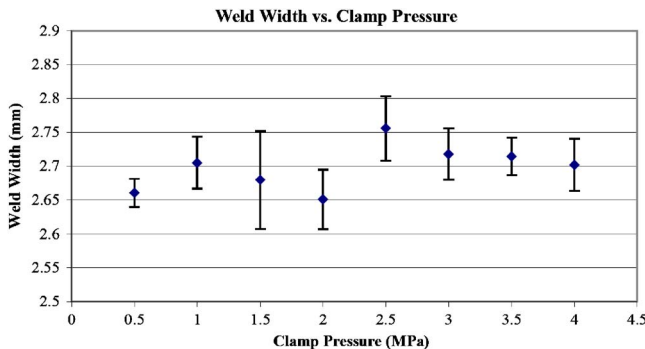


**Fig. 13** Average weld width for each pressure level. The error bars equate to the standard deviation of the mean.

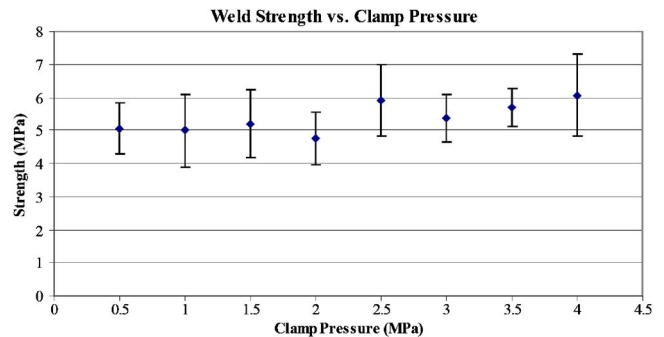


**Fig. 14** Average calculated weld strength as a function of clamping pressure. The error bars in the plot are the standard deviation of the mean.

the factor levels. The data do suggest a slight increase in the weld strength at levels below 2.0 MPa and above 2.5 MPa, yet this difference is not significant when compared to the standard error of each factor level. As discussed previously, similar results were found by Potente when analyzing the weld strength as a function of pressure, and although slight trends could be found in the data, firm conclusions cannot be drawn [11].

It should be noted that the pressure factor discussed in this experiment is the applied clamping pressure, which is not the same as the pressure in the weld zone during welding. The reason for this distinction is that additional pressure is created due to the thermal expansion of the two parts. This additional pressure is a function of the temperature, depth of heating in both materials, and the elastic modulus, which, as discussed in the first paper of this set, is a function of the temperature. To gain a feeling for the actual pressure distribution in the weld zone as a function of time, the reader is referred to the output plots of the model found in the first paper.

Through intuition and by analyzing the inputs to the model discussed in the first paper, one would expect higher quality welds at higher levels of pressure. The visual assessment demonstrates that a certain weld pressure is required to achieve consistent welds. A significant step increase in the weld width was found above a central weld pressure, yet a slight decline appears to occur above 2.5 MPa. The weld strength data did not contribute significant findings to the variation in weld quality as a function of pressure.

Finally, it should be noted that this experiment was run at a single laser power and welding velocity combination. The previous experiment found that the laser power and welding velocity combination used in this experiment did not result in the maximum weld strength. It is possible that at a different combination of laser power and weld velocity the influence of pressure could yield different results. For example, at higher weld velocities, the pressure is expected to have a greater influence on the weld quality because a higher contact conduction is required due to the shorter heating time.

## Conclusion

Two welding experiments were used to fulfill the purpose of validating the laser transmission welding model while providing further insight into the influence of welding parameters on weld quality. These experiments included varying the laser power and welding velocity in a fully crossed  $4 \times 4$  factorial with four replications of each factor level combination and the second experiment varying the clamping pressure across eight levels with eight replications of each level.

The experiment varying power and velocity provided some important conclusions. First, from a visual inspection, a band of "good" welds was formed across a diagonal extending from low power and low velocity to high power and high velocity. Welds formed at high power and low velocity resulted in some form of decomposition, while welds formed at low power and high velocity resulted in thin or tapering welds. The weld width was found to increase with increasing line energy. Similarly, the weld strength generally increased with increasing line energy. In factor level combinations where decomposition occurred, the trend in increasing weld strength was not present.

The most important outcome from the first experiment is validating the model. The weld width predicted by the heating phase model and the measured weld widths in the experiment were compared at 14 different factor level combinations. In the first factor level combination representing the design solution of the first paper of this set, a laser power of 17 W and weld velocity of 0.06 m/s, the predicted weld width was 2.60 mm while the measured weld width was 2.49 mm, an error of 4.3%. For all 14 factor level combinations the average error was 5.6%, which strongly supports the accuracy of the model.

A final important outcome of the first experiment is defining a decomposition temperature. By analyzing the output of the model for a condition exhibiting slight decomposition, an approximate temperature for the onset of decomposition was found. From this analysis it was found that decomposition occurs when the maximum temperature in the bulk of the material is near 948 K and the maximum temperature at the interface between the two parts is near 889 K. Note that these values are for a weld velocity of 0.05 m/s, and are most likely different for different weld velocities as decomposition is a function of time and temperature.

The second experiment of this paper varied the clamping pressure, while keeping the other operating parameters constant. From a visual inspection, significant differences were found in samples welded at different clamping pressures. In samples welded at or below 2.5 MPa, the fraction of samples in each subgroup exhibiting a tapering weld increased with decreasing clamp pressure. At the two lowest levels of clamping pressure three of the eight samples exhibited tapering of the weld across the sample.

The weld width was found to vary with clamping pressure, with a maximum width found at a clamping pressure of 2.5 MPa. A significant increase occurs in the weld width between 2.0 MPa and 2.5 MPa. The strength data from this experiment did suggest a general increase in the weld strength with increasing clamping pressure, but the difference between the factor levels was not significant compared to the standard error. For this reason, no solid conclusions can be made about the weld strength as a function of clamping pressure.

## Acknowledgment

The authors would like to thank Andersen Corporation for generously sponsoring this work. In addition, we would like to thank David Rowley for his assistance in running a portion of the experiments.

## References

- [1] Van de Ven, J., and Erdman, A., 2006, "Laser Transmission Welding of Thermoplastics—Part I: Temperature and Pressure Modeling," *ASME J. Manuf. Sci. Eng.*, **129**, pp. 849–858.
- [2] Becker, F., and Potente, H., 2002, "A Step Towards Understanding the Heating Phase of Laser Transmission Welding in Polymers," *Polym. Eng. Sci.*, **42**(2), pp. 365–374.
- [3] Van de Ven, J., and Erdman, A., 2006, "Near-Infrared Laser Absorption of Polyvinylchloride at Elevated Temperatures," *J. Vinyl Addit. Technol.*, accepted.
- [4] Kennish, Y., Shercliff, H. R., and McGrath, G. C., 2002, "Heat Flow Model for Laser Welding of Polymers," *Proceedings of the Society of Plastics Engineers' Annual Technical Conference*, San Francisco, CA, May 5–9, 1, pp. 1132–1136.
- [5] Baylis, B., Prabhakaran, R., Bates, P., Huang, Y. P., Xu, S. X., and Watt, D., 2003, "Pyrometer Measurements During Laser Welding of Thermoplastic Elastomers to Polypropylene and of Nylon to Itself," *Proceedings of the Society of Plastics Engineers' Annual Technical Conference*, Nashville, TN, May 4–8, 1, pp. 1111–1115.
- [6] Herzog, D., Barcikowski, S., Fargas, M., Hustedt, M., Sattari, R., and Bunte, J., 2004, "Laser Welding of Wood and Natural Fiber Composites with Thermoplastics," *Proceedings Global Wood and Natural Fiber Composites Symposium*, Kassel, Germany, April 27–28.
- [7] Abed, S., Laurens, P., Carretero, C., Deschamps, J. R., and Duval, C., 2001, "Diode Laser Welding of Polymers: Microstructures of the Welded Zones for Polypropylene," *Proceedings Laser Institute of America, 20th International Congress on ICALEO 2001*, Jacksonville, FL, Oct. 15–18, pp. 1499–1507.
- [8] Prabhakaran, R., Kontopoulou, M., Zak, G., Bates, P., and Baylis, B., 2004, "Laser Transmission Welding of Unreinforced Nylon 6," *Proceedings Proceedings of the Society of Plastics Engineers' Annual Technical Conference*, Chicago, IL, May 16–20, 1, pp. 1205–1209.
- [9] Kagan, V. A., and Pinho, G. P., 2004, "Laser Transmission Welding of Semicrystalline Thermoplastics—Part II: Analysis of Mechanical Performance of Welded Nylon," *J. Reinf. Plast. Compos.*, **23**(1), pp. 95–107.
- [10] Kagan, V. A., and Woosman, N. M., 2004, "Efficiency of Clearwelding Technology for Polyamides," *J. Reinf. Plast. Compos.*, **23**(4), pp. 351–359.
- [11] Potente, H., Becker, F., Fiegler, G., and Korte, J., 2001, "Investigations Towards Application of a New Technique on Laser Transmission Welding," *Weld. World*, **45**(5), pp. 2–7.
- [12] Grewell, D., 1999, "Applications with Infrared Welding of Thermoplastics," *Proceedings ANTEC*, New York, 1, pp. 1411–1415.
- [13] Juvinal, R. C., and Marshek, K. M., 2005, *Fundamentals of Machine Component Design*, Wiley, Hoboken, NJ.